Delivery of a novel porous hybrid thermoresponsive hydrogel into the stroke infarct reduces reactive astrogliosis and promotes neural progenitor cell proliferation.

Mozammel H. Bhuiyan[1,2,3,4*], Simon F.R. Hinkley[5], Andrew N. Clarkson[3]

[1]Sir John Walsh Research Institute, Faculty of Dentistry, Division of Health Sciences, University of Otago, Dunedin, New Zealand

[2]Centre for Bioengineering and Nanomedicine, University of Otago, Dunedin, New Zealand

[3]Department of Anatomy, Brain Health Research Centre and Brain Research New Zealand, University of Otago, Dunedin, New Zealand

[4]Department of Physiology and Neuroscience, Zilkha Neurogenetic Institute, Keck Schook of Medicine of USC, Los Angeles, CA, USA

[5]Ferrier Research Institute, Victoria University of Wellington, Wellington 5012, New Zealand

[*]Corresponding author: Mozammel H. Bhuiyan, current address: Department of Physiology and Neuroscience, Zilkha Neurogenetic Institute, Keck Schook of Medicine of USC, 1501 San Pablo Street, Los Angeles, CA, 90033, USA, phone: +1 (213) 469-9820, Email: mbhuiyan@usc.edu.

Keywords: chitosan, glycerophosphate, thermoresponsive hydrogel, stroke, astrogliosis

Abstract

Stroke remains a leading cause of adult disability worldwide mainly due to brain's limited regeneration and repair mechanisms. In the acute and into the chronic phases of ischemic stroke, reactive astrogliosis serves as a major barrier to improvements in neuroplasticity and tissue regeneration. Currently, no therapies are available to regenerate brain tissue lost due to stroke. Here, in a mouse model of photothrombotic stroke, we demonstrate that a hydrogel formulation made from chitosan and β-glycerophosphate as well as hybrid hydrogel formulations developed by combining chitosan, silk fibroin, polyvinyl alcohol, polyvinyl pyrrolidone, and β-glycerophosphate significantly reduce reactive gliosis in the peri-infarct tissue after stroke. We also show that these hybrid hydrogel formulations retain thermoresponsive gelation properties at physiological temperature and are injectable into a stroke cavity *in vivo*. In addition, the hybrid hydrogel formulations were biocompatible, biodegradable and demonstrated desirable porous microstructure characteristics. To the best of our knowledge, this is the first report demonstrating the neuroprotective potential of CS / β-GP-based hydrogels in dampening reactive astrogliosis following stroke, which would allow these hybrid hydrogels to be combined with drug- or cell-based therapies to enhance functional recovery.

1 Introduction

Stroke is a neurological condition characterized by acute focal dysfunction of the brain, retina, or spinal cord, typically caused by a disruption in one of the cerebral arteries (Lo, Dalkara et al. 2003, Hankey 2017). Affecting over 15 million people annually, stroke remains a leading cause of adult mortality and disability worldwide (Organisation 2018). Currently, reperfusion therapies-such as recombinant tissue plasminogen activator (tPA) or mechanical thrombectomy using self-expanding stent retriever - are the only effective pharmacological treatments for stroke (Yang, Zhang et al. 2020, Suzuki, Matsumaru et al. 2021). However, these therapies are only effective when administered within 4 to 6 hours (for tPA) and 12-24 hours (for thrombectomy) after stroke onset (Hacke, Kaste et al. 2008, Lees, Bluhmki et al. 2010, Feske 2012). Due to this narrow therapeutic window, only 5 – 15% of stroke patients benefit from such treatments, leaving many patients living with permanent disabilities.

Whilst reperfusion therapies may restore blood flow; they do not prevent brain tissue degeneration or promote regeneration of damaged brain tissue during the sub-acute to chronic phases following a stroke. During this critical phase, the peri-infarct brain tissue undergoes reorganization, which significantly impacts long-term functional recovery (Yanev, van Tilborg et al. 2022). At present, no clinically approved treatments exist to promote long-term functional recovery after stroke. Therefore,

there is an urgent need to develop novel stroke therapies with broader therapeutic windows and regenerative potential.

Emerging research has demonstrated that biopolymer hydrogels have the capacity to promote long-term brain tissue regeneration in rodent stroke models. These hydrogels have been shown to reduce post-stroke inflammation, facilitate the migration of neural progenitor cells to the lesion site, and allow the sustained release of drugs and neurotrophic factors into the peri-infarct tissue (Nih, Sideris et al. 2017, Nih, Gojgini et al. 2018, Liu, Zhang et al. 2022). Additionally, previous research has demonstrated that biopolymer hydrogels can be injected directly into the infarct cavity in the brain through minimally invasive procedures. Once injected, these hydrogels adapt to the irregular shape of the infarct cavity through *in situ* gelation (Lam, Lowry et al. 2014, Cook, Nguyen et al. 2017, Tuladhar, Obermeyer et al. 2020).

Despite the promise of preclinical studies, biopolymer hydrogel-based treatments have yet to be successfully translated for human use. A significant challenge in clinical translation is the development of biopolymer hydrogels with physicochemical and mechanical properties that closely match those of injured brain tissue, while also retaining their biological functionality. We show that biopolymers have distinct biological properties based on their composition, and this must be tuned to match brain tissue mechanics.

An innovative approach to developing hydrogels for brain implantation involves combining multiple biopolymers into a hybrid or composite hydrogel system and optimizing their ratios based on the mechanical properties of injured tissue. Chitosan (CS) / β-glycerophosphate (β-GP) hydrogels represent promising candidates for injectable delivery into the infarct cavities of the brain due to their thermoresponsive gelation properties, with a lower critical solution temperature (LCST) close to physiological temperature (37ºC) (Zhang, He et al. 2020). Previous studies have investigated CS / β-GP hydrogels alone or in combination with other polymers for regeneration applications in various tissues, such as bone, cartilage, spinal cord and periodontal tissue. Wu et al. demonstrated that implantation of CS / β-GP / silk fibroin hydrogel containing copper and bioactive glass nanoparticles promoted the regeneration of vascularized bone tissue and the deposition of mineralized collagen in a rat model of calvarial bone defects (Wu, Zheng et al. 2019). Similarly, Peng et al. found that CS / β-GP / hyaluronic acid hydrogel loaded with mesenchymal stem cells enhanced cardiac function in a mouse model of myocardial infarction (Peng, Li et al. 2022). Despite these findings, CS / β-GP hydrogels have not yet been investigated for regenerating damaged brain tissue following stroke.

In this study, we propose developing a hybrid hydrogel composed of CS, β-GP, silk fibroin (SF), polyvinyl alcohol (PVA), and polyvinyl pyrrolidone (PVP) to promote the regeneration of brain tissue after a stroke. Previously, we characterized the physicochemical properties and *in vitro* cytotoxicity of

CS / β-GP hydrogels with varying concentrations of CS and β-GP to assess their suitability for injectable neural tissue regeneration applications (Bhuiyan, Clarkson et al. 2023). Our findings revealed that 0.75% w/v CS / 3% w/v β-GP hydrogels exhibited rapid gelation at 37ºC, while supporting the viability and proliferation of PC12 cells *in vitro* - an immortalized cell line with neuronal cell-like properties.

Silk fibroin (SF) is a natural polymer studied previously in our laboratory, where we demonstrated that implanting SF nano-scaffolds into infarct cavities significantly reduced the expression of glial fibrillary acidic protein (GFAP), a marker for reactive astrogliosis, in the peri-infarct tissue (Boni, Ali et al. 2020). Both PVA and PVP are synthetic polymers well known for their biocompatibility and use in biomedical applications (Sali, Gould et al. 2021). These synthetic polymers are frequently incorporated into biopolymer blends to enhance their mechanical and viscoelastic properties (Lei, Cong et al. 2024).

In this study, we blended CS and β-GP with SF, PVA and PVP to develop novel hybrid hydrogel formulations and evaluate their potential for regenerating damaged brain tissue following a stroke. The formulations were comprehensively characterized in terms of their physicochemical properties, including rheological behaviors, morphology, biodegradation, and *in vitro* cytotoxicity to identify the optimal composition for stroke-induced brain tissue regeneration. Subsequently, we implanted the hybrid hydrogel formulations in a mouse model of photothrombotic stroke to assess their effects on post-stroke peri-infarct reactive astrogliosis, microglial reactivity, and proliferation of neural progenitor cells in the sub ventricular zone (SVZ). To the best of our knowledge, this is the first study to evaluate CS and β-GP based hybrid hydrogels for tissue regeneration following a stroke.

2 Results

2.1 Hydrogel design

Hydrogels intended for brain repair following a stroke must have specific properties. They should be injectable through a fine needle to minimize damage to surrounding tissue, exhibit an appropriate gelation time to allow adequate delivery and filling of the infarct cavity, possess a porous structure to support the release of therapeutic agents, and most importantly be biocompatible (Lam, Lowry et al. 2014). To meet these requirements, we designed hybrid hydrogels that are liquid at room temperature (25□) to permit injection and then rapidly transition into a semisolid gel at physiological temperature (37□) to be retained in the infarct cavity post-injection.

In our previous study, we demonstrated that hydrogels composed of 0.5% (w/v) CS / 3% (w/v) β-GP and 0.75% (w/v) CS / 3% (w/v) β-GP are porous, non-cytotoxic, and have suitable thermoresponsive gelation properties for injectable applications (Bhuiyan, Clarkson et al. 2023). Building on this, we developed six hybrid hydrogel formulations by combining 0.75% CS and 3% β-GP with SF, PVA and PVP (**Table 1**). The non-cytotoxic concentrations of SF, PVA and PVP were determined by MTT assay using PC12 cells, an immortalized cell line with neuron-like properties (**Figure S1**). Based on these results, the maximum safe concentrations incorporated into the hybrid hydrogels were 3% for SF, 2% for PVA and 1% for PVP.

Table 1: Composition and characteristics of the hybrid hydrogels

Name of hydrogels	**Concentration (%, w/v)**					**pH**	**Gelation time at 37°C (min)**	**Gelation temp. (°C)**	**Porosity (μm) Mean ± SEM**
	CS	**SF**	**PVA**	**PVP**	**β-GP**				
F1	0.75	-	-	-	3	7.14	5	36	56.3 ± 1.3
F2	0.75	3	-	-	3	7.10	26	39	79.9 ± 4.3
F3	0.75	-	2	-	3	7.07	1	31	35.6 ± 1.1
F4	0.75	-	-	1	3	7.05	3	34	23.0 ± 17.1
F5	0.75	3	2	1	3	7.05	8	39	18.8 ± 19.5
F6	0.75	2	1	0.5	3	7.04	2	36	30.2 ± 16.6

CS: chitosan, SF: silk fibroin, PVA: polyvinyl alcohol, PVP: polyvinyl pyrrolidone, β-GP: sodium β-glycerophosphate.

2.2 Viscoelastic and thermoresponsive properties of the hybrid hydrogels

The viscoelastic behavior and mechanical properties of the hybrid hydrogels were characterized using a dynamic frequency sweep test (Zhou, Dai et al. 2021). The storage modulus (G′) represents the elastic (solid-like) response of the material to an external force, while the loss modulus (G") reflects its viscous (liquid-like) response. When G′ is greater than G", the material exhibits a solid-like behavior; conversely, when G" is greater, the material behaves more like a liquid. Frequency sweep tests were conducted after 1 h of incubation at 37°C to allow sufficient time for gelation. As shown in Figure 1A, G′ was consistently higher than G" at low frequencies for all hybrid hydrogels, indicating a stable, solid-like state. As the frequency increased G′ decreased sharply while G" remained relatively unchanged, suggesting that the hybrid hydrogels exhibit oscillatory shear thinning behaviors. This shear-thinning property may be advantageous for injectable applications. Notably, the

addition of 2% PVA to 0.75% CS / 3% β-GP (formulation F3) increased G′ at low frequencies, indicating enhanced mechanical strength. In contrast, the incorporation of 3% SF or 1% PVP (formulations F2 and F4, respectively) decreased G′ at low frequencies, suggesting a reduction in mechanical strength. Combining all three polymers (2% PVA, 1% PVP and 2% SF) with 0.75% CS / 3% β-GP (formulation F5) further reduced G′ at low frequencies. However, when the concentrations of SF, PVA and PVP were lowered to 2%, 1%, and 0.5% respectively and combined with 0.75% CS / 3% β-GP (formulation F6), G’ increased compared to F5. Still, the mechanical strength of F6 remained lower than that of F1 and F3.

The thermoresponsive nature and gelation temperature of the hybrid hydrogels were assessed using a temperature sweep test (**Figure 1A**). At 25°C, all formulations exhibited low G′ and G" values, indicating liquid-like behavior at room temperature. A sharp increase in G′ as the temperature approached the gelation temperature. Gelation temperature is defined as the temperature at which G′ surpasses G" marking the transition from a liquid to a gel state (Cho, Heuzey et al. 2006, Dang, Yan et al. 2011). Gelation temperatures for each formulation are summarized in **Table 1**. The 0.75% CS / 3% β-GP hydrogel (F1) gelled at 36□. SF raised the gelation temperature to 39°C, indicating that SF delays gelation. In contrast, incorporating 2% PVA (F3) and 1% PVP (F4) lowered the gelation temperatures to 31°C and 34°C, respectively, suggesting that these additives promote earlier gelation. The formulation containing all three additives (F5) exhibited a gelation temperature of 39°C. This increase implies that the higher combined polymer content may interfere with the CS-β-GP interactions necessary for efficient gelation. To address this, the concentrations of SF, PVA and PVP were reduced to 2%, 1% and 0.5%, respectively in formulation F6. This adjustment resulted in a decreased gelation temperature to 36°C, aligning more closely with that of the base formulation (F1).

2.3 Gelation time of the hybrid hydrogels

The hybrid hydrogels were designed to retain their temperature-induced gelation properties close to physiological temperature and pH. Gelation time was measured using the inverted test tube method at 37°C, and the results are summarized in **Table 1**. The base formulation of 0.75% CS / 3% β-GP (F1) exhibited a gelation of 5 min. The addition of 3% SF increased the gelation time to 26 min (F2), while the inclusion of 2% PVA (F3) and 1% PVP (F4) reduced the gelation times to 1 min and 3 min, respectively. When all three polymers - 3% SF, 2% PVA and 1% PVP - were combined in a single formulation (F5), gelation time increased to 8 min. However, reducing the concentrations to 2% SF, 1% PVA and 0.5% PVP in formulation F6, significantly shortened the gelation time to 2 min. These findings were further validated using a rheological time sweep test, as shown in **Figure 1A**.

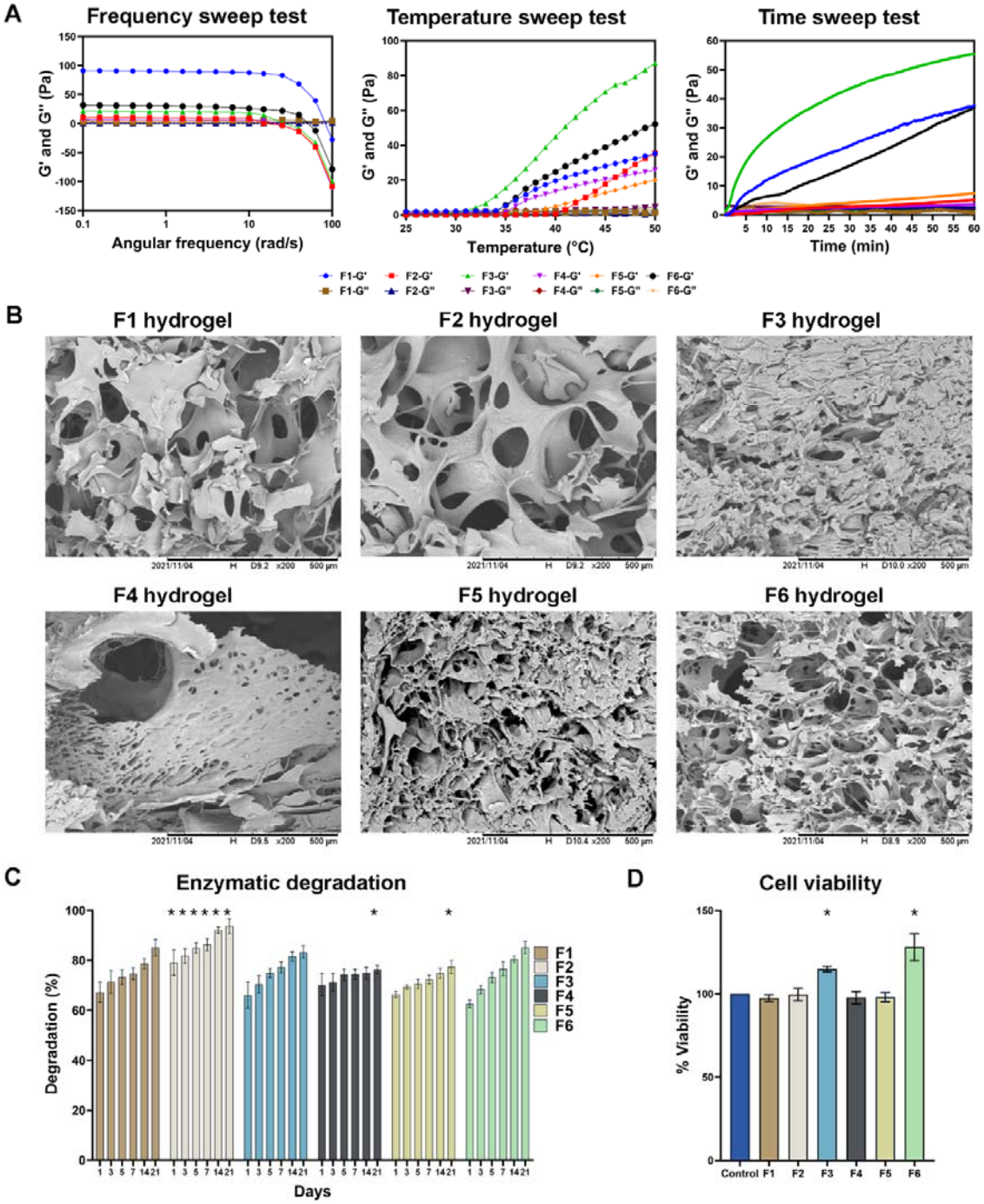

Figure 1: Physical and biological characterization of hybrid hydrogel formulations. A) Frequency sweep, temperature sweep and time sweep tests of hybrid hydrogels. B) SEM image of the surface morphology of hybrid hydrogels. C) Enzymatic degradation of hybrid hydrogels. Data are expressed as mean ± SEM for n = 3. Data were analyzed by Two-way ANOVA followed by Tukey's test for post-hoc comparisons. Asterisks (*) represented significant values. D) Cell viability of PC12 cells grown inside hybrid hydrogels after 24 h. Data are

expressed as mean ± SD for n = 3. Data were analyzed by one-way ANOVA followed by Tukey's test for post-hoc comparisons. Asterisks (*) represented significant values. F1: 0.75% chitosan / 3% β-GP, F2: 0.75% chitosan / 3% β-GP/ 3% SF, F3: 0.75% chitosan / 3% β-GP/ 2% PVA, F4: 0.75% chitosan / 3% β-GP/ 1% PVP, F5: 0.75% chitosan / 3% β-GP/ 3% SF / 2% PVA / 1% PVP, F6: 0.75% chitosan / 3% β-GP/ 2% SF / 1% PVA / 0.5% PVP.

2.4 Fourier transform infrared (FTIR) characterization of the hybrid hydrogels

The chemical interactions among CS, SF, PVA, PVP and β-GP were investigated using FTIR spectroscopy (**Figure S2)**. The FTIR spectrum of pure CS showed a broad shoulder between 3400-3200 cm^{-1}, corresponding to O-H stretching overlapped with the N-H stretching. Peaks at 2909 and 2868 cm^{-1} indicating C-H stretching, while peaks at 1641 cm^{-1} (C=O bending), 1587 cm^{-1} (N-H bending), and 1418 cm^{-1} ($C-CH_3$ symmetric deformation) were also observed, in agreement with previous reports (Ke, Li et al. 2020). Pure SF displayed characteristic peaks at 1582 and 1509 cm^{-1}, corresponding to C=O stretching and N-H bending associated with β-sheet structures. An additional peak at 1235 cm^{-1} was attributed to C-N and N-H vibrations from random coil and α-helix structures (Boni, Ali et al. 2020). The FTIR spectrum of pure PVA showed a broad peak between 3450-3200 cm^{-1}, corresponding to O-H stretching, peaks at 2940 and 2908 cm^{-1} for C-H stretching from alkyl groups, and a prominent peak at 1140 $cm^{-1}$for C-O stretching. For pure PVP, characteristic peaks included a strong C=O stretch (amide I) at 1655 cm^{-1} , aromatic to C-H deformation at 1490 and 1458 cm^{-1}, C-N stretching in the pyrrolidone structure at 1288 cm^{-1} (Ata, Rasool et al. 2020).

In the hybrid hydrogels, characteristic peaks of CS were retained, with a shift in the O-H stretching band in F2 due to SF incorporation. Minor shifts at 1647, 1587, and 1418 cm□¹ indicated interactions with other polymers (**Figure S2a**). SF-specific peaks were observed in F2, F5, and F6 hydrogels, with the C=O peak shifting from 1582 to 1592 cm□¹ and N–H bending shifting from 1509 to 1516 cm□¹ (F2) and 1523 cm□¹ (F5 and F6; **Figure S2b**). Similarly, PVA peaks were identifiable in F3, F5 (**Figure S2c**), and F6, and PVP peaks were evident in F4, F5, and F6 with minor shifts indicating polymer–polymer interactions (**Figure S2d**).

2.5 Morphology of the hybrid hydrogels

The interior morphology and porosity of the hybrid hydrogel were examined using scanning electron microscopy (SEM) after lyophilization at -80°C. SEM images in **Figure 1B** revealed variations in pore size and structure depending on the type and concentrations of incorporated biopolymers. The F1 hydrogel exhibited a smooth microstructure with regular pores and sheet-like layers. Incorporation of 3% SF (F2) significantly increased the pore size and resulted in a rougher microstructure. Conversely, the addition of 2% PVA (F3) and 1% PVP (F4) reduced pore size and compacted the sheet-like. The

combined inclusion of 3% SF, 2% PVA and 1% PVP (F5) led to a further reduction in pore size compared to F1-F4. Interestingly, lowering the incorporations to 2% SF, 1% PVA and 0.5% PVP (F6) increased pore size relative to F5.

2.6 Enzymatic biodegradation of the hybrid hydrogels

Upon injection, hydrogels are expected to degrade through enzymatic hydrolysis. To assess this, *in vitro* biodegradation studies were conducted using lysozyme-containing PBS solution at 37°C over 1, 3, 5, 7, 14, and 21 days. All formulations showed a time-dependent increase in degradation (**Figure 1C)**. Two-way ANOVA comparisons revealed that F2 (3% SF) exhibited significantly higher degradation rates than F1 at all time points: day 1, 3, 5, 7, and 14 ($P \leq 0.0001$), and 21 days ($P \leq 0.01$). F3 (2% PVA) did not show significant differences from F1. In contrast, F4 (1% PVP) showed slightly reduced degradation, with a significant decrease at day 21 ($P \leq 0.001$). A similar trend was observed in F5 (SF + PVA + PVP), which also showed significantly lower degradation on day 21 ($P \leq 0.01$). F6 showed slightly reduced degradation at day 1 but followed a similar degradation profile to F1 at later time points.

2.7 Cytotoxicity of the hybrid hydrogels

Cytotoxicity of the hybrid hydrogels was evaluated using the MTT assay after 24 hours of co-culture with PC12 cells. As shown in **Figure 1D,** all hybrid hydrogels maintained over 90% cell viability, indicating good biocompatibility. One-way ANOVA analysis revealed significantly increased in cell viability in F3 ($P \leq 0.01$) and F6 ($P \leq 0.0001$) compared to the cell-only control. No significant difference in cell viability were found for F1, F2, F4, or F5 relative to the control.

2.8 Effect of hybrid hydrogels on infarct volume after ischemic stroke

The *in vivo* regenerative potential of hybrid hydrogels were evaluated using a mouse model ischemic stroke induced by photothrombosis as described previously (Clarkson, Huang et al. 2010). Mice received a systemic injection of Rose Bengal, a photosensitive dye, followed by cortical illumination to produce reactive oxygen species and localized platelet aggregation. This method induces a focal stroke without reperfusion, leading to a small cortical infarct with partially salvageable penumbra that evolves over 2–3 days (Hilger, Blunk et al. 2004). Based on prior findings (Clarkson, López-Valdés et al. 2013) hybrid hydrogels were injected into the infarct cavity 5 days post-stroke to allow full lesion

maturation. Fourteen days post-stroke, infarct volume was assessed using cresyl violet (CV) staining (**Figure 2**). Photothrombosis produced a distinct focal lesion in the primary motor cortex of the left hemisphere (**Figure 2a**). Slight reductions in average infarct volume were observed in F2, F3, and F6 groups. However, one-way ANOVA analysis revealed no statistically significant differences among treatment groups (F□,□□ = 0.2717, P = 0.8930).

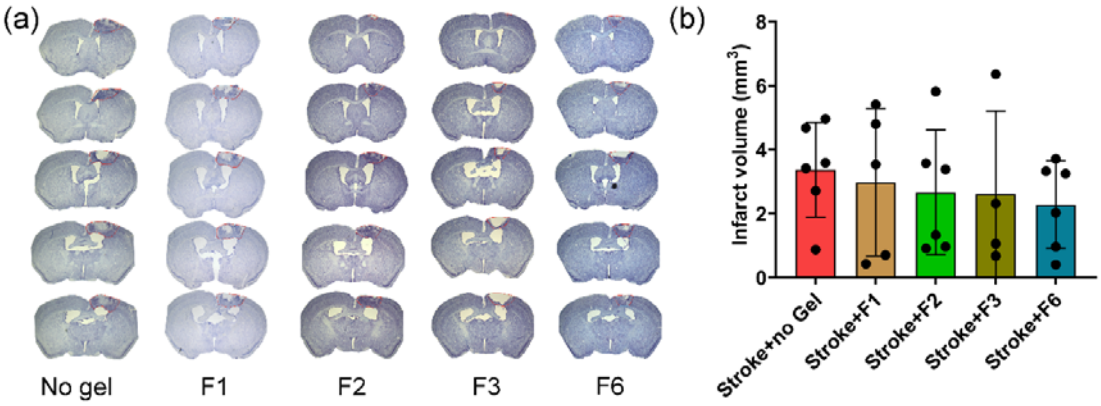

Figure 2: Quantification of infarct volumes 2 weeks post-stroke. (a) Representative Cresyl violet stained images of coronal sections at 14-day after stroke from all treatment groups: stroke + no gel, n = 6; stroke + F1, n = 5; stroke + F2, n = 6; stroke + F3, n = 4; and stroke + F6, n = 6. (b) Quantification of infarct volumes at 14-days after stroke. Data are expressed as mean ± SD and black dots represent individual animals. Data were analyzed by one-way ANOVA followed by Tukey's post-hoc comparisons.

2.9 Effect of hybrid hydrogels on stroke-induced reactive astrogliosis

Stroke leads to morphological changes in astrocytes including proliferation and hypertrophy, a process known as reactive astrogliosis (Sofroniew 2014). This phenomenon contributes to glial scar formation in the peri-infarct region. We examined the effect of hybrid hydrogels on stroke-induced reactive astrogliosis two weeks post-stroke, as shown in **Figure 3**. The expression of glial fibrillary acidic protein (GFAP) is a well-established marker of reactive astrogliosis (Lamtahri, Hazime et al. 2021, Houlton, Zubkova et al. 2022). In this study, GFAP expression was quantified in cortical layers 2/3 and 5 of both the peri-infarct and lateral (distal) regions. Stroke increased GFAP expression in the peri-infarct region 2 weeks post-stroke, with a noticeable decrease in expression in more lateral regions. One-way ANOVA analysis revealed significant differences in GFAP expression between treatment groups in both layer 2/3 ($F_{4, 22}$ = 4.345, P = 0.0097) and layer 5 ($F_{4,22}$ = 7.560, P = 0.0005). Notably, the F6 hydrogel significantly decreased GFAP expression in the peri-infarct region of both layers 2/3 (P = 0.0098) and 5 (P = 0.0007). A similar reduction was observed in the F2 hydrogel in both layers 2/3 (P = 0.0249) and 5 (P = 0.0037). The F1 hydrogel demonstrated a significant effect

only in layer 5 (P = 0.0036), while the F3 hydrogel did not produce significant effects in either layer (layer 2-3: P = 0.0632; layer 5: P = 0.1994). The GFAP expression in the lateral cortex was consistent across all treatment groups (**Figure S3**).

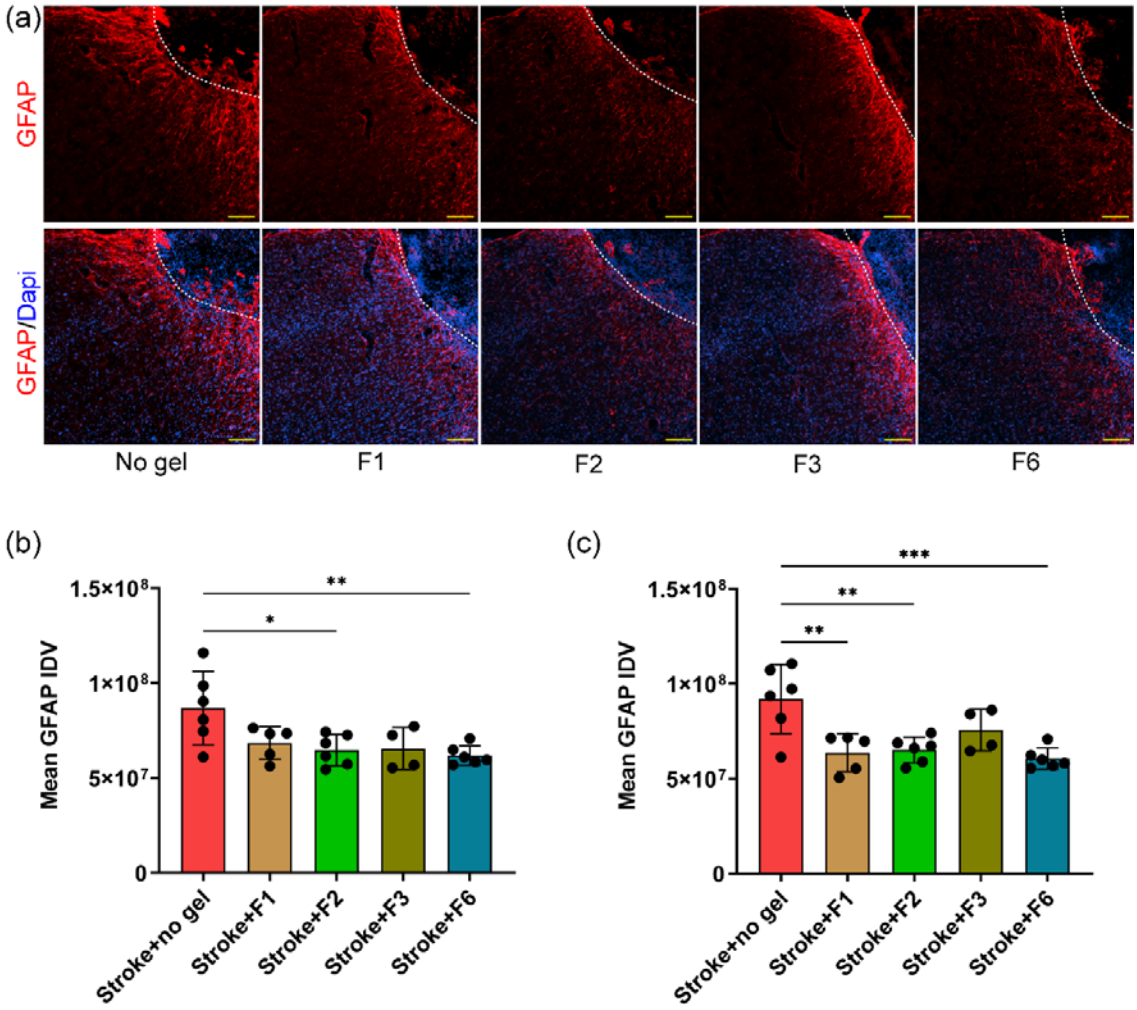

Figure 3: Stroke-induced reactive astrogliosis 2 weeks post-stroke. (a) Representative fluorescent images of GFAP (+ve) astrocytes (shown in red) in the peri-infarct area at 2-weeks after stroke from all treatment groups: stroke + no gel, n = 6; stroke + F1, n = 5; stroke + F2, n = 6; stroke + F3, n = 4; and stroke + F6, n = 6. Scale bar = 50 µm. All sections have been counter stained with DAPI (shown in blue). Quantification of mean integrated density values (IDV) of GFAP (+ve) astrocytes at (b) the cortical layer 2/3 peri-infarct, and (c) cortical layer 5 peri-infarct. Data are expressed as mean ± SD and black dots represent individual animals. Data were analyzed by one-way ANOVA with Tukey's test for post hoc comparisons. Asterisks (*) represented the significant values, * = $P \leq 0.05$, ** = $P \leq 0.01$, and *** = $P \leq 0.001$.

2.10 Effect of hybrid hydrogels on stroke-induced microglial activation

We next investigated the effects of hybrid hydrogels on microglial activation two weeks post-stroke, as shown in **Figure 4**. Under normal conditions, microglia play a role in immune surveillance and maintaining brain homeostasis (Nimmerjahn, Kirchhoff et al. 2005). However, following a stroke, microglia become activated – undergoing hypertrophy and developing thickened processes – resulting in a state termed microgliosis (Zhang 2019). Activated microglia accumulates in the peri-infarct region, promoting a proinflammatory response that worsens stroke pathology during the subacute phase (Hu, Leak et al. 2015, Zhao, Ma et al. 2017). To evaluate microglial activation, we quantified the expression of ionized calcium-binding adapter molecule 1 (Iba1), a commonly used microglial marker (Nih, Sideris et al. 2017), in cortical layers 2/3 and 5 of the peri-infarct area. Similar to GFAP, Iba1 expression was markedly upregulated in the peri-infarct region two weeks post-stroke, with a decreased expression observed in lateral cortical regions. One-way ANOVA revealed significant differences among groups in both cortical layer 2/3 ($F_{4, 22} = 4.014$, $P = 0.0136$) and layer 5 ($F_{4, 22} = 3.007$, $P = 0.0403$). Treatment with the F2 hydrogel significantly reduced the Iba1 expression in peri-infarct layer 2/3 ($P = 0.0217$), while the F6 hydrogel significantly reduced the expression in layer 5 ($P = 0.0321$) compared to stroke + no gel controls. No decrease in Iba1 expression was observed in F1 (layers 2/3: $P = 0.3463$, and layers 5: $P = 0.6141$) or F3 (layers 2/3: $P = 0.6141$, and layers 5: $P = 0.6436$) hydrogel groups.

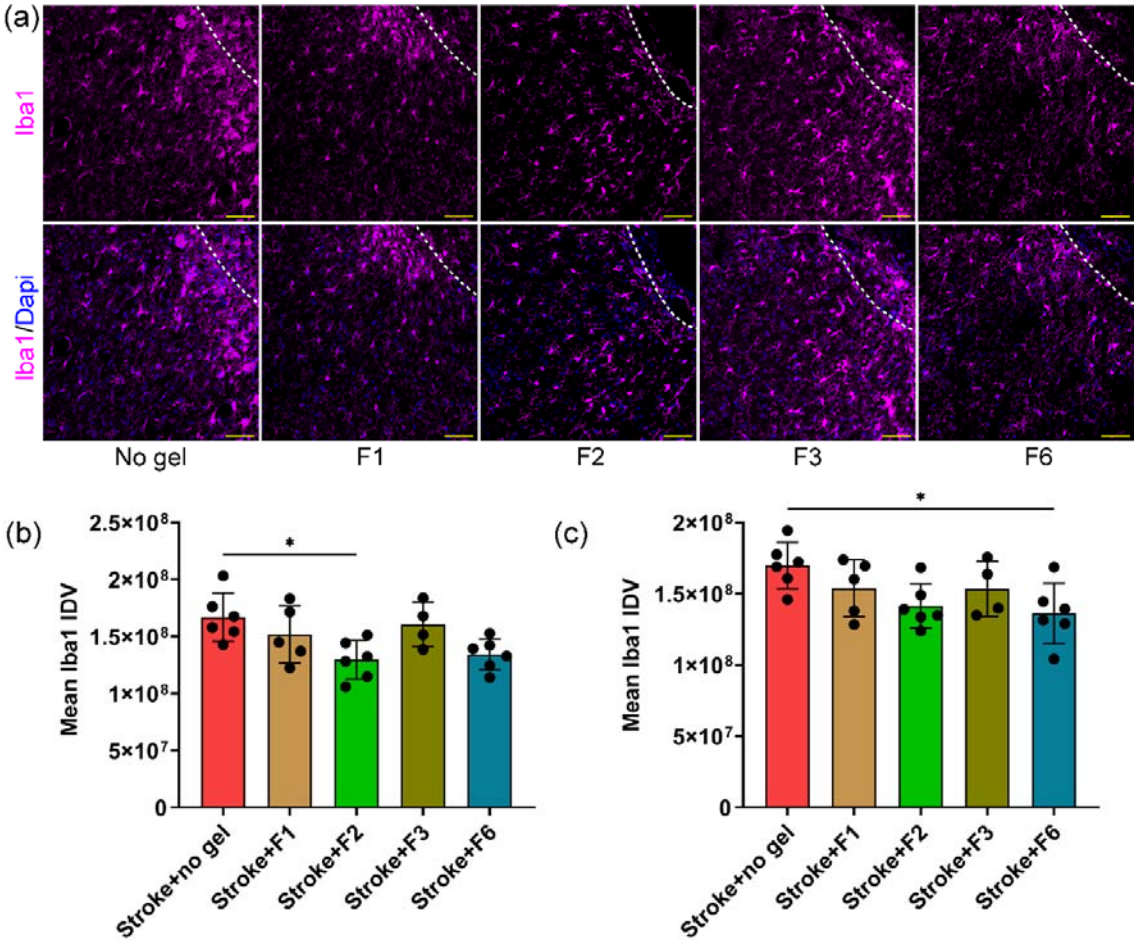

Figure 4: Stroke-induced microglial activation 2 weeks post-stroke. (a) Representative fluorescent images of Iba1 (+ve) microglia (shown in purple) in the peri-infarct area at 2-weeks after stroke from all treatment groups: stroke + no gel, n = 6; stroke + F1, n = 5; stroke + F2, n = 6; stroke + F3, n = 4; and stroke + F6, n = 6. Scale bar = 50 µm. All sections have been counter stained with DAPI (shown in blue). Quantification of mean integrated density values (IDV) of Iba1 (+ve) microglial cells at (b) the cortical layer 2/3 peri-infarct, and (c) cortical layer 5 peri-infarct. Data are expressed as mean ± SD and black dots represent individual animals. Data were analyzed by one-way ANOVA with Tukey's test for post hoc comparisons. Asterisks (*) represented the significant values, * = $P < 0.05$.

2.11 Effect of hybrid hydrogels on post-stroke neurogenesis

Following the assessment of both astrogliosis and microglial activation, we next evaluated the effects of hybrid hydrogels on post-stroke neurogenesis in the subventricular zone (SVZ). In the adult brain, neurogenesis occurs primarily in the SVZ and dentate gyrus. After stroke, neuroblasts in the SVZ proliferate and migrate towards the infarct area. However, most fail to reach the stroke core due to poorly understood inhibitory mechanisms (Thored, Arvidsson et al. 2006). In the present study, we assessed neuroblast proliferation in the ipsilateral SVZ by quantifying the expression of doublecortin (DCX), a neuroblast marker, as shown in **Figure 5**. One-way ANOVA indicated a significant

difference in DCX expression among groups ($F_{4, 22}$ = 6.976, P = 0.0009). Treatment with the F2 hydrogel led to increase in DCX expression compared to the Stroke + no gel control group (P = 0.0001). Similarly, F1 (P = 0.0485) and F6 (P = 0.0157) hydrogels also significantly enhanced DCX expression. The F3 hydrogel did not produce a difference in DCX-expression compared to the Stroke + no gel control group (P = 0.0735).

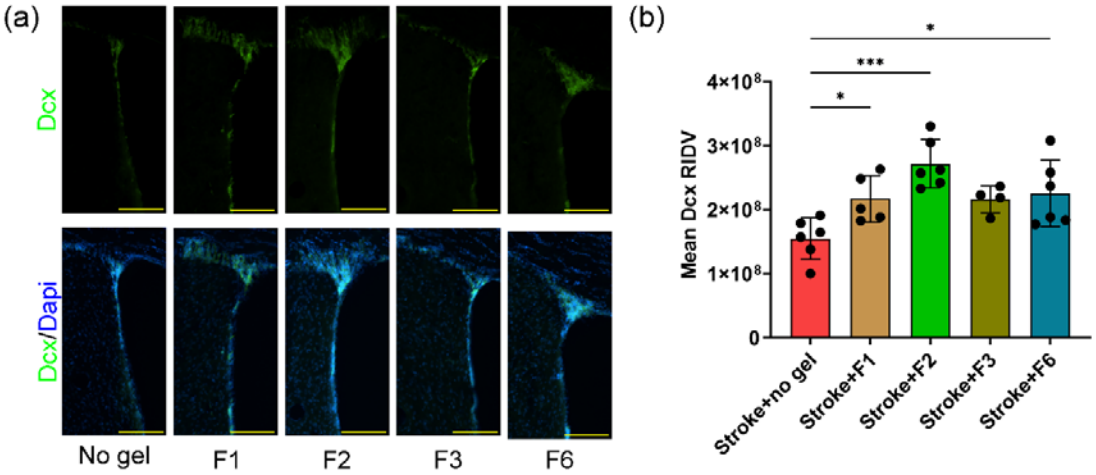

Figure 5: Neurogenesis 2 weeks post-stroke. (a) Representative fluorescent images of Dcx (+ve) neuroblasts (shown in green) at ipsilateral sub-ventricular zone (SVZ) at 14-day after stroke from all treatment groups: stroke + no gel, n = 6; stroke + F1 hydrogel, n = 5; stroke + F2, n = 6; stroke + F3, n = 4; and stroke + F6, n = 6. Scale bar = 100 µm. All sections have been counter stained with DAPI (shown in blue). (b) Quantification of raw integrated density values (RIDV) of Dcx (+ve) neuroblasts at ipsilateral SVZ. Data are expressed as mean ± SD and black dots represent individual animals. Data were analyzed by one-way ANOVA with Tukey's test for post hoc comparisons. Asterisks (*) represented the significant values, * = P ≤ 0.05, *** = P ≤ 0.001.

3 Discussion

This study aimed to design novel hybrid hydrogel formulations using biopolymers such as CS, β-GP, SF, PVA and PVP, and evaluate their therapeutic potentials in a mouse model of photothrombotic stroke. CS is a highly biocompatible polymer, and CS / β-GP hydrogels have been shown to support various tissues (Zhou, Jiang et al. 2015). In particular, the lower critical solution temperature (LCST) and shear-thinning properties of CS / β-GP hydrogels make them suitable candidates for injectable applications (Bhuiyan, Clarkson et al. 2023). While CS / β-GP hydrogels have been used in tissue engineering, their potential for brain tissue regeneration after stroke had not been investigated. SF exhibits excellent biocompatibility and contains RGD motifs, which enhance cellular interactions (Kang, Wang et al. 2018). In addition, both PVA and PVP are commonly used in tissue engineering due to their favorable viscoelastic and mechanical properties (Kumar and Han 2017, Vedadghavami, Minooei et al. 2017).

Thermoresponsive hydrogels with an LCST close to physiological temperature are ideal candidates for *in vivo* injectable applications. Additionally, rapid gelation is essential to prevent material diffusion into surrounding tissues. In this study, F1 (0.75% CS / 3% β-GP) hydrogel exhibited temperature-induced gelation near physiological temperature. This behavior is attributed to electrostatic and hydrophobic interactions between CS and β-GP along with hydrogen bonding between the phosphate groups of β-GP and amine groups of CS (Zhou, Jiang et al. 2015). The incorporation of multiple biopolymers affected the gelation time and temperature. For example, the F2 hydrogel (0.75% CS / 3% SF / 3% β-GP) exhibited and increased gelation temperature, while F3 (0.75% CS / 2% PVA / 3% β-GP) and F4 (0.75% CS / 1% PVP / 3% β-GP) hydrogels exhibited decreased gelation temperatures. This suggests that SF promoted the phase transition at higher temperatures, whereas PVA and PVP favored the phase transition at lower temperatures. Notably, PVA and PVP improved the mechanical properties of F3 and F4 hydrogels, respectively, as indicated by an increased storage modulus, G′ compared to the F1 and F2 hydrogels. When all three biopolymers, SF, PVA and PVP were combined with CS into a single formulation, the F5 hydrogel (0.75% CS / 3% SF / 2% PVA / 1% PVP / 3% β-GP), gelation temperature and time increased, but mechanical properties decreased, suggesting that the excessive presence of biopolymers weakened the CS / β-GP interactions. In the F6 hydrogel (0.75% CS / 2% SF / 1% PVA / 0.5% PVP / 3% β-GP), both gelation temperature and mechanical properties were improved by reducing the concentration of each biopolymer. This was consistent with previous studies, which reported that CS / SF / β-GP hydrogels exhibit weaker mechanical properties (Wu, Zheng et al. 2019). In contrast, when CS / SF / β-GP was combined with glass nanoparticles, enhanced mechanical properties of the composite hydrogels were observed, making them suitable for bone tissue engineering. However, this hydrogel is not appropriate for brain tissue regeneration as softer materials are preferred (Hopkins, Laura et al. 2013). For this, we show that blending the CS / SF / β-GP with PVA and PVP improved mechanical properties without compromising thermoresponsive behaviors.

The porosity of hydrogels plays a critical role in cellular infiltration and diffusion of therapeutics required for neurite extension through the hydrogel microstructure (Gerecht, Townsend et al. 2007). Previous studies have shown that microporous hyaluronic acid hydrogels can reduce glial scar formation and inflammatory responses after stroke (Nih, Sideris et al. 2017). In this study, Nih and colleagues showed that microporous hydrogels decreased glial scar formation, whereas nanoporous hydrogels with similar composition failed to demonstrate any effect. In our study, all hybrid hydrogels displayed interconnected microporous structures. Based on the findings by Nih et al., this suggests that the microporous structure of the hybrid hydrogels contributes to preventing glial scar formation after stroke (**Figure 3**). A notable difference among the hydrogels was a significant difference in the average pore diameter. SF decreased crosslinking density, resulting in larger pores in the F2 hydrogel, while PVA and PVP increased crosslinking and decreased pore size in F3, F4, F5, and F6 hydrogels.

Degradation of hydrogels is crucial for clinical translation to ensure safe removal of implanted materials from the body (Biran, Martin et al. 2005). The use of non-biodegradable material for brain implants is not desirable as these can result in chronic inflammation and impair function and recovery (Aurand, Lampe et al. 2012), which is why investigating biodegradation kinetics is essential. CS is metabolized by lysozyme into non-toxic metabolites, D-glucosamine and N-acetyl-D-glucosamine (Yang, Li et al. 2010), which are both components of the extracellular matrix. In the present study, all hybrid hydrogels except F5 demonstrated stable degradation, with over 70% degradation within 21 days in PBS containing lysozyme. Han et al. (2004) reported similar degradation rates for CS / β-GP-hydrogels with approximately 80% degradation within 50 days in vivo, following subcutaneous injection, further supporting our findings (Han, Nam et al. 2004).

For *in vitro* cytotoxicity, PC12 cells, which resemble neurons, have previously been used to assess the safety of hydrogels and neuroprotective potential of biomaterials (Hussain, Javorina et al. 2006, Green, Lovell et al. 2009, Mehri, Abnous et al. 2012). Assessments revealed that all hybrid hydrogels supported the growth of PC12 cells, indicating no cytotoxicity and therefore safe to use. Interestingly, F3 and F6 hydrogels showed a significant increase in cell growth, suggesting that PVA may have a bioactive effect on PC12 cells (**Figure 1D**). However, further studies are needed to elucidate how PVA may influence cell growth and proliferation.

Based on the physicochemical characterization and *in vitro* cytotoxicity studies, we can summarize that: (1) F1, F2, F3, F4 and F6 hydrogels showed suitable gelation and mechanical properties, (2) F1, F2, F3 and F6 hydrogels have a porous structure suitable for cell growth and infiltration, (3) F1, F2, F3, F5 and F6 hydrogels showed stable biodegradation kinetics, and (4) none of the hydrogels showed any significant *in vitro* cytotoxicity. After considering these results, F1, F2, F3 and F6 hydrogels were selected for *in vivo* studies to evaluate biocompatibility and effects on brain tissue regeneration following stroke.

Two weeks after stroke, we observed a lesion in the primary motor cortex, with similar infarct volumes across all treatment groups, indicating that the hydrogels had no effect on the infarct volume (**Figure 2**). From the lack of any exacerbating effects of the gels on infarct size, we can infer *in vivo* biocompatibility.

Assessment of GFAP expression revealed a significant decrease in the peri-infarct region for F1, F2 and F6 hydrogel-treated mice, indicating reduced reactive astrogliosis (**Figure 3**). The decrease in GFAP expression across the hydrogels is likely attributed to different components of the gels: CS for F1 hydrogel, combined CS and SF for F2 hydrogel, and mechanical properties and SF for F6 hydrogel. These findings align with our previous report, where SF nanoscaffolds reduced reactive astrogliosis two weeks post-stroke (Boni, Ali et al. 2020). To extend previous hydrogel findings, we

show for the first time that CS / β-GP hydrogel can also decrease reactive astrogliosis 2 weeks post-stroke. The presence of reactive astrocytes after stroke produces chondroitin sulfate proteoglycans, ephrin-A5, and other inhibitory molecules in the peri-infarct region that inhibit axonal sprouting and neural plasticity that is required for post-stroke functional recovery (Hill, Jin et al. 2012, Overman, Clarkson et al. 2012). Therefore, pharmacological agents that decrease peri-infarct reactive astrogliosis are being trialed preclinically and shown to promote functional recovery (Bix, Gowing et al. 2013, Lamtahri, Hazime et al. 2021, Houlton, Zubkova et al. 2022). Therefore, to further advance the hydrogels used in the present studies, follow-up long-term behavioral studies are warranted.

Further to a decrease in reactive astrogliosis, a significant reduction in Iba1 expression in layer 2/3 of the peri-infarct region was observed for the F2 hydrogel, suggesting that SF may play a role in decreasing microglial activation. We believe that this decrease in microglial activation was linked to SF as the F1 hydrogel that only contains CS, failed to decrease microglial activation. In contrast, treatment with F6 hydrogel decreased Iba1 expression in layer 5 of the peri-infarct area, which could be attributed to SF. These findings are consistent with previous studies demonstrating the ability of SF to decrease microglial activation 3 weeks after MCAO stroke in rats (Gorenkova, Osama et al. 2019). Excessive microglial activation during the sub-acute phase after stroke exacerbates functional recovery after stroke (Planas 2024), so dampening microglial activation could facilitate functional recovery, although further studies are required, as well as follow-up studies investigating F2 or F6 hydrogel to promote functional recovery following stroke.

Finally, treatment with either F1, F2, or F6 hydrogels were found to promote neurogenesis in the SVZ (**Figure 5**). Interestingly, the F1 hydrogel without any growth factor or biological signaling molecule enhanced neurogenesis. It is possible that the RGD motifs in SF are likely contributing to neurogenesis, as SF hydrogels have been shown to promote neural regeneration (Boni, Ali et al. 2020, Chang, Cho et al. 2021). González-Pérez et al. also reported that hydrogels containing RGD-sequence can promote neurogenesis at 2-, 4- and 6 weeks after spinal cord injury (González-Pérez, Alonso et al. 2022). This study further extends our understanding of CS / β-GP hydrogel, which we show also supports neurogenesis after stroke.

4 Conclusion

Biopolymer hydrogels, with or without additional bioactive molecules, have been extensively studied as a therapeutic strategy for brain repair following stroke. In the present study, we have developed hybrid hydrogels by combining CS, SF, PVA, PVP and β-GP that can be delivered into the brain via slow infusion for the treatment of ischemic stroke. The hybrid hydrogels (F1, F3 and F5)

demonstrated gelation at physiological temperature, microporous structure, and biodegradation kinetics suitable for in vivo applications. The in vivo study demonstrated that the hybrid hydrogels, particularly F2 and F6, modulate reactive astrogliosis, reduce microglial activation, and enhance neurogenesis in a mouse model of stroke. These findings suggest that local hydrogel delivery can improve the post-stroke brain environment and support neural regeneration. However, further research is necessary to evaluate the long-term effects on functional recovery after stroke.

5 Experimental section

Materials: CS (Mw: 503 kDa, degree of deacetylation: 91%) was purchased from Shanghai Waseta International Trading Company, China. The molecular weight and degree of deacetylation of CS were characterized using gel permeation chromatography (Agilent PL-GPC 50) and FT-IR spectroscopy, respectively (Rajabi, Cabral et al. 2022). PVA powder (degree of hydrolysis: 99% hydrolyzed, Mw: 89-98 kDa) and PVP powder (Mw: 360 kDa), β-glycerol phosphate disodium salt pentahydrate (Mw: 306.11 kDa), lysozyme from chicken egg white, 3-(4,5-dimethylthiazol-2-yl)-2,5-diphenyltetrazolium bromide (MTT), dimethyl sulfoxide (DMSO), and acetic acid were purchased from Sigma Aldrich, New Zealand. Silk fibroin (Mw: 300 kDa) was obtained from Xi'an Herbking Biotechnology Company (Gaoxin District, Xi'an 710075, China) in powder form.

Preparation of CS, SF, PVA, PVP and β-GP stock solutions: In order to prepare hybrid hydrogel formulations, stock solutions for each biomaterial were prepared as follows: CS 3% w/v, SF 20% w/v, PVA 10% w/v, PVP 10% w/v and β-GP 50% w/v. To prepare CS stock solution, CS was weighed and dissolved in 0.8% (v/v) acetic acid by stirring for 24 h using a magnetic stirrer at room temperature (25°C) to prepare homogenous solutions. To prepare SF and β-GP stock solutions, SF and β-GP were weighed and dissolved in deionized water separately by stirring for 4 h using a magnetic stirrer at 25°C. To prepare PVA and PVP stock solutions, PVA and PVP were weighed and dissolved in deionized water separately by stirring for 4 h using a magnetic stirrer at 80°C.

Preparation of hybrid hydrogels: A predetermined volume of stock solution for each biopolymer was mixed in different ratios to prepare hybrid biomaterial solutions as described in **Table 1**. The hybrid biomaterial and β-GP stock solutions were then kept in an ice bath for at least 30 min to cool down to ~ 4°C. The cold β-GP stock solution was then added dropwise to the hybrid biomaterial solutions to make the final β-GP concentration to 3% w/v with continuous stirring for at least 1 h using a magnetic stirrer to prepare hybrid hydrogel solutions as mentioned in **Table 1**. The final volume of hybrid hydrogel solutions was adjusted by addition of deionized water. The

temperature of the system was maintained at ~ 4°C during the whole process. Finally, the pH was measured using a pH meter (pH 209, Hanna Instruments, USA).

Gelation time: Gelation time of the hybrid hydrogels was determined by the inverted tube test as described previously (Huang, Chen et al. 2016). Briefly, the hydrogel forming solution for each hydrogel was added to a transparent glass vial and incubated in a 37 °C water bath. The viscosity of the solution was monitored every 30 s by inverting the tubes horizontally. The time at which the solution stopped flowing was recorded as the gelation time.

Rheological properties: Rheological properties of the hybrid hydrogels were investigated using an oscillatory rheometer (Discovery HR-3, TA Instruments) equipped with a cone and plate geometry of 2° and 60 mm in diameter. Freshly prepared hydrogel-forming solutions were used for the rheological analysis. An oscillatory stress sweep test was performed from 0.1 to 10 Pa with a frequency of 0.1, 1, 10, and 50 Hz at 37 °C to confirm that the frequency and strain were within the linear viscoelastic region (LVR). A frequency sweep test was performed for each hydrogel from 0.1 to 100 rad/s at a constant stress of 1 Pa and at 37 °C. Based on these test results, a stress of 1 Pa and a frequency of 1 Hz was chosen for temperature sweep and time sweep tests. A temperature sweep test from 25 to 50 °C at a heating rate of 1 °C/min and a time sweep test at 37 °C for 60 min were performed for each hydrogel with a constant frequency of 1 Hz and stress of 1 Pa to determine the effect of temperature and time, respectively, on the storage modulus (G') and loss modulus (G") of hybrid hydrogels. The G' represents the elastic property and describes the solid-state behavior, whereas G" characterizes the viscous property as seen with the liquid-state behavior of the sample. The temperature and time at which the G' value crossed the G" value is considered gelation temperature and gelation time, respectively.

Fourier transform infrared (FTIR) spectroscopy: The FTIR spectroscopy (ALPHA FTIR, Bruker, USA) was used to characterize the chemical bonds present in the hybrid hydrogels. The spectrums were obtained in ATR mode over the wavelength range between 400 – 4000 cm^{-1} with a spectral resolution of 4 cm^{-1}.

Morphology: The surface morphology along with porosity of the hybrid hydrogels was observed by scanning electron microscopy (SEM) (model: TM3030, Hitachi) as previously described (Pettinelli, Rodríguez-Llamazares et al. 2019). The freeze-dried hydrogel samples were coated with palladium-gold using an Emitech K575X Peltier-cooled high-resolution sputter coater (EM Technologies Ltd., Kent, England) prior to analysis. The coated samples were viewed at an accelerating voltage of 15 kV. The pore diameter was assessed by measuring Feret's diameter of 6 pores in three randomly selected sections in each SEM micrograph.(Sali, Gould et al. 2021)

Enzymatic biodegradation: The enzymatic biodegradation was measured Gravimetrically as described previously (Sudheesh Kumar, Srinivasan et al. 2011). Briefly, a small cube-shaped sample of freeze-dried hydrogels was cut (1 cm^3), weighed (W_i), and immersed in PBS (pH 7.4) containing lysozyme (2 µg/ml) at 37 °C for 1, 3, 5, 7, 14, and 21 days. At each time point, the samples were removed from the enzymatic media, freeze-dried and weighed (W_t). Enzymatic degradation was assessed using the following formula:

$$\text{Degradation (\%)} : \frac{W_i - W_t}{W_i} \times 100$$

Cytotoxicity testing: The cytotoxicity was assessed using MTT assay on PC12 cells (PC12, catalogue no. CRL-1721, ATCC). Briefly, PC12 cells were seeded in 96-well plates at a density of 1 x 10^4 cells/ml per well in RPMI media (Gibco) supplemented with 10% fetal bovine serum (FBS, Gibco) and 1% penicillin- streptomycin. Following cell adhesion, either of PBS (control), β-GP, biopolymer and hybrid hydrogel solutions were added to the wells in triplicate (**Table 1**). The cells were then incubated for 24 h in an incubator (Heracell VIOS 160i, Thermo Scientific) at 37 °C and 5% CO_2. Subsequently, media containing testing solutions was replaced by media containing MTT (0.4 mg/ml) and incubated for another 4 h. Following incubation, MTT containing media was removed and formazan was dissolved with DMSO. Finally, absorbance was measured at 550 nm using a microplate reader (SpectraMax i3x MultiMode Detection Platform, Molecular Devices, USA). The average absorbance of control PBS-exposed cells was considered as 100% cell viability with average change in absorbance of β-GP solution or HFS treated wells measured to calculate cell viability (%).

Animals and surgical procedures: All animal procedures were carried out in accordance with the guidelines on the care and use of laboratory animals as approved by the University of Otago Animal Ethics Committee (AUP# AUP-19-170). The experimental groups were randomized and blinded according to recommendations from the Stroke Therapy Academic Industry Roundtable (STAIR), Stroke Recovery and Rehabilitation Roundtable (SRRR) and Animal Research: Reporting of In Vivo Experiments (ARRIVE) guidelines for all behavioral and histological assessments (Fisher, Feuerstein et al. 2009, Corbett, Carmichael et al. 2017, Percie du Sert, Hurst et al. 2020). Male C57BL/6 mice, aged between 2-3 months, body weights between 25-30 g were housed under a 12h light/dark cycle with ad libitum access to food and water. Focal cerebral infarction was induced using the photothrombotic method as described previously (Clarkson, Huang et al. 2010). In brief, under isoflurane anesthesia (2 – 2.5% in O_2), mice were placed in a stereotaxic apparatus. The skull was then exposed through a midline incision and underlying connective tissue and periosteum were cleared and dried. A cold light source (3300KW, Scott, LCD) attached to a 20x objective, giving a 2

mm diameter illumination, was positioned 1.5 mm left from bregma and 0.2 ml Rose Bengal solution (Sigma Aldrich, 10 mg/ml in normal saline) was administered intraperitoneally. After 5 min, the brain was illuminated through the intact skull for 15 min, creating an infarction in the primary motor cortex (Clarkson, Huang et al. 2010). The body temperature was maintained at 36.9 ± 0.2°C using a rectal probe attached to a homeothermic blanket during the whole procedure (Harvard Apparatus, Massachusetts, USA).

Intracerebral implantation of hydrogel: On day 5 post-stroke, mice were anesthetized and placed in a stereotaxic apparatus. The skull was exposed through a midline incision and cleaned as described before. A small bur hole was created in the skull over the stroke region and 8µl of hydrogel solution (either of F1, F2, F3, F6) was injected into the infarct cavity using a 30-gauge needle attached to a Hamilton syringe (Hamilton®, USA) connected to a pump with an infusion rate of 1 µl/min. The needle was withdrawn 1 min after the injection and the skin glued back together using surgical glue.

Mouse tissue processing and immunohistochemistry: Fourteen days following stroke, mice were anesthetized and intracardially perfused with 4% paraformaldehyde solution (PFA). The brains were immediately collected and postfixed for an hour in 4% PFA before being transferred to 30 % sucrose solution in PBS. Brains were cut into 30 µm thick coronal sections using a freezing stage sledge microtome (Leitz Wetzlar, Germany) and the sections were stored in cryoprotectant at – 20°C.

Infarct volume: Infarct volume was determined by histological assessment using Cresyl violet staining, as previously described.(Li, Zheng et al. 2005, Shirazi, Vyssotski et al. 2022) For each animal, every sixth section throughout the coronal plane was stained with Cresyl violet and digitized using Stereo Investigator software (Microbrightfield). The edges of the core of the infarct were defined using the drawing tool of Fiji ImageJ (version: 1.53q, National Institute of Health, USA) and the area of the selected regions were measured by an observer blinded to the animal's treatment groups. Infarct volume was then quantified as follows:

$$\text{Infarct volume (mm}^3\text{)} = \text{Area (mm}^2\text{) x Section thickness (mm) x Section interval}$$

Immunohistochemistry: Every twelfth section was rinsed in tris – buffered saline (TBS) at room temperature. Next, they were incubated in a blocking solution (**Table 2**) for 60 min with continuous shaking (60 rpm) at room temperature. The sections were then incubated in the primary antibody solution (**Table 2**) at 4°C for 48 h with continuous shaking (60 rpm). Sections were then rinsed in TBS before being kept in the secondary antibody solution (**Table 2**) for 2 h at room temperature. Following subsequent rinsing in TBS, sections were incubated in Hoechst solution for 10 min. Following incubation with Hoechst solution, sections were rinsed in TBS and subsequently

mounted onto gelatine-coated glass slides, air-dried, passed sequentially through alcohol (50%, 70%, 95%, 100%) and xylene, before being coverslipped using DPX mounting solution.

Table 2: Composition of blocking buffer, primary and secondary antibody solutions

	Blocking buffer	**Primary antibody solution**	**Secondary antibody solution**
GFAP staining	5% NGS, catalogue no. G9023, Sigma Aldrich), 0.3% w/v Triton X-100 in 0.05 M TBS solution	Polyclonal chicken anti-GFAP antibody (dilution 1:2000, catalogue no. AB5541, Sigma Aldrich), 2% NGS, and 0.3% w/v Triton X-100 in 0.05M TBS solution	Goat anti-chicken Dylight® 488 antibody (dilution 1:400, catalogue no. ab96947, Abcam), 2% NGS, and 0.3% w/v Triton X-100 in 0.05 M TBS solution
Iba1 staining	5% NDS, catalogue no. ab7475, Abcam), 0.3% w/v Triton X-100 in 0.05 M TBS solution	polyclonal rabbit anti-Iba1 antibody (dilution 1:800, catalogue no. 019-19741, Fujifilm Wako Pure Chemical Corporation, Japan), 2% NDS, and 0.3% w/v Triton X-100 in 0.05 M TBS solution	Donkey anti-rabbit Dylight® 550 antibody (dilution 1:800, catalogue no. ab96892, Abcam), 2% NDS, and 0.3% w/v Triton X-100 in 0.05 M TBS solution
Dcx staining	5% NDS, 0.3% w/v Triton X-100 in 0.05 M TBS solution	polyclonal goat anti-Dcx antibody (dilution 1:400, catalogue no. sc-8066, Santa Cruz Biotechnology), 2% NDS, and 0.3% w/v Triton X-100 in 0.05 M TBS solution	Donkey anti-goat Dylight® 549 antibody (dilution 1:800, catalogue no. 705-505-147, Jackson ImmunoResearch Lab Inc.), 2% NDS, and 0.3% w/v Triton X-100 in 0.05 M TBS solution

NGS: normal goat serum, NDS: normal donkey serum, GFAP: glial fibrillary acidic protein, Iba1: Ionized calcium-binding adaptor molecule 1, Dcx: Doublecortin.

Image analysis: Photomicrographs of the sections were taken using an inverted microscope (Eclipse Ti2, Nikon, Japan). To quantify the expression of GFAP and Iba1, the integrated density value (IDV) was quantified across four regions of interests (ROIs, 200 µm x 200 µm): (1) cortical layer 2/3 peri-infarct, (2) cortical layer 5 peri-infarct, (3) cortical layer 2/3 lateral (approximately 600 µm apart from peri-infarct regions), (4) cortical layer 5 lateral, using Fiji ImageJ software. To quantify the expression of Dcx, the raw integrated density value (RIDV) of the subventricular zone, wall of the lateral ventricle was quantified using Fiji ImageJ software.

Statistical Analyses: The group size for each experiment was determined by a power analysis based on previous similar studies and animals were randomly assigned to different experimental groups (Clarkson, Huang et al. 2010, Trout, Kahle et al. 2021). The experimental groups were blinded

according to recommendations from the Stroke Therapy Academic Industry Roundtable (STAIR), Stroke Recovery and Rehabilitation Roundtable (SRRR) and Animal Research: Reporting of In Vivo Experiments (ARRIVE) guidelines for all behavioral and histological assessments (Fisher, Feuerstein et al. 2009, Corbett, Carmichael et al. 2017, Percie du Sert, Hurst et al. 2020).

Statistical analyses were done using GraphPad Prism 9 (GraphPad software Inc., San Diego, USA). Differences between the porosity of hybrid hydrogels were evaluated by one-way analysis of variance (ANOVA). The difference between enzymatic biodegradation of hybrid hydrogels was analyzed by two-way ANOVA. Tukey's multiple comparison test was used to further investigate any significant effect observed. Quantification of infarct volume and immunohistochemical analyses were also assessed by one-way ANOVA and Tukey's multiple comparison test was conducted to further investigate any significant effect observed. A confidence interval of $P < 0.05$ was considered statistically significant. All bar graphs are presented as mean ± standard deviation (SD) unless otherwise stated.

6 Conflict of interest

The authors declare no conflict of interest.

7 Funding information

This project was funded by the University of Otago Doctoral Scholarship paid to Mozammel H. Bhuiyan and a funding from the Ministry of Business, Innovation and Employment, New Zealand.

8 Authors contribution

MHB: conceptualization, methodology, investigation, analysis, writing-original first draft & editing; SFRH: writing-review & editing; ANC: conceptualization, supervision, visualization, writing-review & editing.

9 References

Ata, S., A. Rasool, A. Islam, I. Bibi, M. Rizwan, M. K. Azeem, A. u. R. Qureshi and M. Iqbal (2020). "Loading of Cefixime to pH sensitive chitosan based hydrogel and investigation of controlled release kinetics." International Journal of Biological Macromolecules **155**: 1236-1244.

Aurand, E. R., K. J. Lampe and K. B. Bjugstad (2012). "Defining and designing polymers and hydrogels for neural tissue engineering." Neuroscience Research **72**(3): 199-213.

Bhuiyan, M. H., A. N. Clarkson and M. A. Ali (2023). "Optimization of thermoresponsive chitosan/β-glycerophosphate hydrogels for injectable neural tissue engineering application." Colloids and Surfaces B: Biointerfaces **224**: 113193.

Biran, R., D. C. Martin and P. A. Tresco (2005). "Neuronal cell loss accompanies the brain tissue response to chronically implanted silicon microelectrode arrays." Experimental Neurology **195**(1): 115-126.

Bix, G. J., E. K. Gowing and A. N. Clarkson (2013). "Perlecan domain V is neuroprotective and affords functional improvement in a photothrombotic stroke model in young and aged mice." Translational Stroke Research **4**(5): 515-523.

Boni, R., A. Ali, S. G. Giteru, A. Shavandi and A. N. Clarkson (2020). "Silk fibroin nanoscaffolds for neural tissue engineering." Journal of Materials Science: Materials in Medicine **31**(9): 81.

Chang, Y., B. Cho, E. Lee, J. Kim, J. Yoo, J.-S. Sung, Y. Kwon and J. Kim (2021). "Electromagnetized gold nanoparticles improve neurogenesis and cognition in the aged brain." Biomaterials **278**: 121157.

Cho, J., M.-C. Heuzey, A. Bégin and P. J. Carreau (2006). "Chitosan and glycerophosphate concentration dependence of solution behaviour and gel point using small amplitude oscillatory rheometry." Food Hydrocolloids **20**(6): 936-945.

Clarkson, A. N., B. S. Huang, S. E. MacIsaac, I. Mody and S. T. Carmichael (2010). "Reducing excessive GABA-mediated tonic inhibition promotes functional recovery after stroke." Nature **468**(7321): 305-309.

Clarkson, A. N., H. E. López-Valdés, J. J. Overman, A. C. Charles, K. C. Brennan and S. Thomas Carmichael (2013). "Multimodal examination of structural and functional remapping in the mouse photothrombotic stroke model." Journal of Cerebral Blood Flow & Metabolism **33**(5): 716-723.

Cook, D. J., C. Nguyen, H. N. Chun, I. L Llorente, A. S. Chiu, M. Machnicki, T. I. Zarembinski and S. T. Carmichael (2017). "Hydrogel-delivered brain-derived neurotrophic factor promotes tissue repair and recovery after stroke." Journal of Cerebral Blood Flow & Metabolism **37**(3): 1030-1045.

Corbett, D., S. T. Carmichael, T. H. Murphy, T. A. Jones, M. E. Schwab, J. Jolkkonen, A. N. Clarkson, N. Dancause, T. Weiloch, H. Johansen-Berg, M. Nilsson, L. D. McCullough and M. T. Joy (2017). "Enhancing the Alignment of the Preclinical and Clinical Stroke Recovery Research Pipeline: Consensus-Based Core Recommendations From the Stroke Recovery and Rehabilitation Roundtable Translational Working Group." Neurorehabilitation and Neural Repair **31**(8): 699-707.

Dang, Q. F., J. Q. Yan, J. J. Li, X. J. Cheng, C. S. Liu and X. G. Chen (2011). "Controlled gelation temperature, pore diameter and degradation of a highly porous chitosan-based hydrogel." Carbohydrate Polymers **83**(1): 171-178.

Feske, S. K. (2012). "Thrombolytic therapy of acute stroke." Circulation **125**(21): 2662-2666.

Fisher, M., G. Feuerstein, D. W. Howells, P. D. Hurn, T. A. Kent, S. I. Savitz and E. H. Lo (2009). "Update of the Stroke Therapy Academic Industry Roundtable Preclinical Recommendations." Stroke **40**(6): 2244-2250.

Gerecht, S., S. A. Townsend, H. Pressler, H. Zhu, C. L. E. Nijst, J. P. Bruggeman, J. W. Nichol and R. Langer (2007). "A porous photocurable elastomer for cell encapsulation and culture." Biomaterials **28**(32): 4826-4835.

González-Pérez, F., M. Alonso, I. González de Torre, M. Santos and J. C. Rodríguez-Cabello (2022). "Protease-Sensitive, VEGF-Mimetic Peptide, and IKVAV Laminin-Derived Peptide Sequences within Elastin-Like Recombinamer Scaffolds Provide Spatiotemporally Synchronized Guidance of Angiogenesis and Neurogenesis." Advanced Healthcare Materials **11**(22): 2201646.

Gorenkova, N., I. Osama, F. P. Seib and H. V. O. Carswell (2019). "In Vivo Evaluation of Engineered Self-Assembling Silk Fibroin Hydrogels after Intracerebral Injection in a Rat Stroke Model." ACS Biomaterials Science & Engineering **5**(2): 859-869.
Green, R. A., N. H. Lovell and L. A. Poole-Warren (2009). "Cell attachment functionality of bioactive conducting polymers for neural interfaces." Biomaterials **30**(22): 3637-3644.
Hacke, W., M. Kaste, E. Bluhmki, M. Brozman, A. Dávalos, D. Guidetti, V. Larrue, K. R. Lees, Z. Medeghri, T. Machnig, D. Schneider, R. von Kummer, N. Wahlgren and D. Toni (2008). "Thrombolysis with Alteplase 3 to 4.5 Hours after Acute Ischemic Stroke." New England Journal of Medicine **359**(13): 1317-1329.
Han, H. D., D. E. Nam, D. H. Seo, T. W. Kim, B. C. Shin and H. S. Choi (2004). "Preparation and biodegradation of thermosensitive chitosan hydrogel as a function of pH and temperature." Macromolecular Research **12**(5): 507-511.
Hankey, G. J. (2017). "Stroke." The Lancet **389**(10069): 641-654.
Hilger, T., J. A. Blunk, M. Hoehn, G. Mies and P. Wester (2004). "Characterization of a Novel Chronic Photothrombotic Ring Stroke Model in Rats by Magnetic Resonance Imaging, Biochemical Imaging, and Histology." Journal of Cerebral Blood Flow & Metabolism **24**(7): 789-797.
Hill, J. J., K. Jin, X. O. Mao, L. Xie and D. A. Greenberg (2012). "Intracerebral chondroitinase ABC and heparan sulfate proteoglycan glypican improve outcome from chronic stroke in rats." Proceedings of the National Academy of Sciences **109**(23): 9155-9160.
Hopkins, A. M., D. L. Laura, T. Federico, S. Elise, S. Cristian, A. T. J., H. J. A. and K. D. L. (2013). "Silk Hydrogels as Soft Substrates for Neural Tissue Engineering." Advanced Functional Materials **23**(41): 5140-5149.
Houlton, J., O. V. Zubkova and A. N. Clarkson (2022). "Recovery of Post-Stroke Spatial Memory and Thalamocortical Connectivity Following Novel Glycomimetic and rhBDNF Treatment." International Journal of Molecular Sciences **23**(9): 4817.
Hu, X., R. K. Leak, Y. Shi, J. Suenaga, Y. Gao, P. Zheng and J. Chen (2015). "Microglial and macrophage polarization—new prospects for brain repair." Nature Reviews Neurology **11**(1): 56-64.
Huang, C. L., Y. B. Chen, Y. L. Lo and Y. H. Lin (2016). "Development of chitosan/beta-glycerophosphate/glycerol hydrogel as a thermosensitive coupling agent." Carbohydrate Polymers **147**: 409-414.
Hussain, S. M., A. K. Javorina, A. M. Schrand, H. M. Duhart, S. F. Ali and J. J. Schlager (2006). "The Interaction of Manganese Nanoparticles with PC-12 Cells Induces Dopamine Depletion." Toxicological Sciences **92**(2): 456-463.
Kang, Z., Y. Wang, J. Xu, G. Song, M. Ding, H. Zhao and J. Wang (2018). "An RGD-Containing Peptide Derived from Wild Silkworm Silk Fibroin Promotes Cell Adhesion and Spreading." Polymers **10**(11): 1193.
Ke, X., M. Li, X. Wang, J. Liang, X. Wang, S. Wu, M. Long and C. Hu (2020). "An injectable chitosan/dextran/β -glycerophosphate hydrogel as cell delivery carrier for therapy of myocardial infarction." Carbohydrate Polymers **229**: 115516.
Kumar, A. and S. S. Han (2017). "PVA-based hydrogels for tissue engineering: A review." International Journal of Polymeric Materials and Polymeric Biomaterials **66**(4): 159-182.
Lam, J., W. E. Lowry, S. T. Carmichael and T. Segura (2014). "Delivery of iPS-NPCs to the Stroke Cavity within a Hyaluronic Acid Matrix Promotes the Differentiation of Transplanted Cells." Advanced Functional Materials **24**(44): 7053-7062.
Lamtahri, R., M. Hazime, E. K. Gowing, R. Y. Nagaraja, J. Maucotel, M. Alasoadura, P. P. Quilichini, K. Lehongre, B. Lefranc, K. Gach-Janczak, A.-B. Marcher, S. Mandrup, D. Vaudry, A. N. Clarkson, J. Leprince and J. Chuquet (2021). "The Gliopeptide ODN, a Ligand for the Benzodiazepine Site of $GABA_A$ Receptors, Boosts Functional Recovery after Stroke." The Journal of Neuroscience **41**(33): 7148-7159.
Lees, K. R., E. Bluhmki, R. von Kummer, T. G. Brott, D. Toni, J. C. Grotta, G. W. Albers, M. Kaste, J. R. Marler, S. A. Hamilton, B. C. Tilley, S. M. Davis, G. A. Donnan, W. Hacke, K. Allen, J. Mau, D. Meier, G. del Zoppo, D. A. De Silva, K. S. Butcher, M. W. Parsons, P. A. Barber, C. Levi, C. Bladin and G. Byrnes (2010). "Time to treatment with intravenous alteplase and outcome in stroke: an

updated pooled analysis of ECASS, ATLANTIS, NINDS, and EPITHET trials." Lancet **375**(9727): 1695-1703.
Lei, L., R. Cong, Y. Ni, X. Cui, X. Wang, H. Ren, Z. Wang, M. Liu, J. Tu and L. Jiang (2024). "Dual-Functional Injectable Hydrogel for Osteoarthritis Treatments." Advanced Healthcare Materials **13**(5): 2302551.
Li, S., J. Zheng and S. T. Carmichael (2005). "Increased oxidative protein and DNA damage but decreased stress response in the aged brain following experimental stroke." Neurobiology of Disease **18**(3): 432-440.
Liu, Y., F. Zhang, L. Long, J. Li, Z. Liu, C. Hu, X. Chen, X. Zan, J. Xu and Y. Wang (2022). "Dual-function hydrogels with sequential release of GSK3β inhibitor and VEGF inhibit inflammation and promote angiogenesis after stroke." Chemical Engineering Journal **433**: 133671.
Lo, E. H., T. Dalkara and M. A. Moskowitz (2003). "Mechanisms, challenges and opportunities in stroke." Nature Reviews Neuroscience **4**(5): 399-415.
Mehri, S., K. Abnous, S. H. Mousavi, V. M. Shariaty and H. Hosseinzadeh (2012). "Neuroprotective Effect of Crocin on Acrylamide-induced Cytotoxicity in PC12 cells." Cellular and Molecular Neurobiology **32**(2): 227-235.
Nih, L. R., S. Gojgini, S. T. Carmichael and T. Segura (2018). "Dual-function injectable angiogenic biomaterial for the repair of brain tissue following stroke." Nature Materials **17**(7): 642-651.
Nih, L. R., E. Sideris, S. T. Carmichael and T. Segura (2017). "Injection of Microporous Annealing Particle (MAP) Hydrogels in the Stroke Cavity Reduces Gliosis and Inflammation and Promotes NPC Migration to the Lesion." Advanced Materials **29**(32).
Nimmerjahn, A., F. Kirchhoff and F. Helmchen (2005). "Resting Microglial Cells Are Highly Dynamic Surveillants of Brain Parenchyma in Vivo." Science **308**(5726): 1314-1318.
Organisation, W. H. (2018). Global Health Estimates 2016: Deaths by Cause, Age, Sex, by Country and by Region, 2000-2016. Geneva, World Health Organization (WHO).
Overman, J. J., A. N. Clarkson, I. B. Wanner, W. T. Overman, I. Eckstein, J. L. Maguire, I. D. Dinov, A. W. Toga and S. T. Carmichael (2012). "A role for ephrin-A5 in axonal sprouting, recovery, and activity-dependent plasticity after stroke." Proceedings of the National Academy of Sciences **109**(33): E2230-E2239.
Peng, L., M. Li, K. Zhao, C. Ma, H. Tang and Y. Li (2022). "Evaluation of an Injectable Hydrogel Based on Hyaluronic Acid–Chitosan/β-Glycerophosphate-Loaded Mesenchymal Stem Cells in Enhancing the Therapeutic Efficacy of Myocardial Infarction." Macromolecular Bioscience **22**(4): 2100286.
Percie du Sert, N., V. Hurst, A. Ahluwalia, S. Alam, M. T. Avey, M. Baker, W. J. Browne, A. Clark, I. C. Cuthill, U. Dirnagl, M. Emerson, P. Garner, S. T. Holgate, D. W. Howells, N. A. Karp, S. E. Lazic, K. Lidster, C. J. MacCallum, M. Macleod, E. J. Pearl, O. H. Petersen, F. Rawle, P. Reynolds, K. Rooney, E. S. Sena, S. D. Silberberg, T. Steckler and H. Würbel (2020). "The ARRIVE guidelines 2.0: Updated guidelines for reporting animal research." Br J Pharmacol **177**(16): 3617-3624.
Pettinelli, N., S. Rodríguez-Llamazares, V. Abella, L. Barral, R. Bouza, Y. Farrag and F. Lago (2019). "Entrapment of chitosan, pectin or κ-carrageenan within methacrylate based hydrogels: Effect on swelling and mechanical properties." Materials Science and Engineering: C **96**: 583-590.
Planas, A. M. (2024). "Role of microglia in stroke." Glia **72**(6): 1016-1053.
Rajabi, M., J. Cabral, S. Saunderson and M. A. Ali (2022). "Green synthesis of chitooligosaccharide-PEGDA derivatives through aza-Michael reaction for biomedical applications." Carbohydrate Polymers: 119884.
Sali, S., M. L. Gould, M. Qasim and A. Ali (2021). "Biodegradable Methacrylated Casein for Cardiac Tissue Engineering Applications." Journal of Materials Chemistry B.
Shirazi, R. S., M. Vyssotski, K. Lagutin, D. Thompson, C. MacDonald, V. Luscombe, M. Glass, K. Parker, E. K. Gowing, D. B. G. Williams and A. N. Clarkson (2022). "Neuroprotective activity of new Δ3-N-acylethanolamines in a focal ischemia stroke model." Lipids **57**(1): 17-31.
Sofroniew, M. V. (2014). "Astrogliosis." Cold Spring Harbor perspectives in biology **7**(2): a020420-a020420.

Sudheesh Kumar, P. T., S. Srinivasan, V.-K. Lakshmanan, H. Tamura, S. V. Nair and R. Jayakumar (2011). "β-Chitin hydrogel/nano hydroxyapatite composite scaffolds for tissue engineering applications." Carbohydrate Polymers **85**(3): 584-591.
Suzuki, K., Y. Matsumaru, M. Takeuchi, M. Morimoto, R. Kanazawa, Y. Takayama, Y. Kamiya, K. Shigeta, S. Okubo, M. Hayakawa, N. Ishii, Y. Koguchi, T. Takigawa, M. Inoue, H. Naito, T. Ota, T. Hirano, N. Kato, T. Ueda, Y. Iguchi, K. Akaji, W. Tsuruta, K. Miki, S. Fujimoto, T. Higashida, M. Iwasaki, J. Aoki, Y. Nishiyama, T. Otsuka, K. Kimura and S. S. Investigators (2021). "Effect of Mechanical Thrombectomy Without vs With Intravenous Thrombolysis on Functional Outcome Among Patients With Acute Ischemic Stroke: The SKIP Randomized Clinical Trial." The Journal of the American Medical Association **325**(3): 244-253.
Thored, P., A. Arvidsson, E. Cacci, H. Ahlenius, T. Kallur, V. Darsalia, C. T. Ekdahl, Z. Kokaia and O. Lindvall (2006). "Persistent Production of Neurons from Adult Brain Stem Cells During Recovery after Stroke." STEM CELLS **24**(3): 739-747.
Trout, A. L., M. P. Kahle, J. M. Roberts, A. Marcelo, L. de Hoog, J. A. Boychuk, S. L. Grupke, A. Berretta, E. K. Gowing, C. R. Boychuk, A. A. Gorman, D. N. Edwards, I. Rutkai, I. J. Biose, H. Ishibashi-Ueda, M. Ihara, B. N. Smith, A. N. Clarkson and G. J. Bix (2021). "Perlecan Domain-V Enhances Neurogenic Brain Repair After Stroke in Mice." Translational Stroke Research **12**(1): 72-86.
Tuladhar, A., J. M. Obermeyer, S. L. Payne, R. C. W. Siu, S. Zand, C. M. Morshead and M. S. Shoichet (2020). "Injectable hydrogel enables local and sustained co-delivery to the brain: Two clinically approved biomolecules, cyclosporine and erythropoietin, accelerate functional recovery in rat model of stroke." Biomaterials **235**: 119794.
Vedadghavami, A., F. Minooei, M. H. Mohammadi, S. Khetani, A. Rezaei Kolahchi, S. Mashayekhan and A. Sanati-Nezhad (2017). "Manufacturing of hydrogel biomaterials with controlled mechanical properties for tissue engineering applications." Acta Biomaterialia **62**: 42-63.
Wu, J., K. Zheng, X. Huang, J. Liu, H. Liu, A. R. Boccaccini, Y. Wan, X. Guo and Z. Shao (2019). "Thermally triggered injectable chitosan/silk fibroin/bioactive glass nanoparticle hydrogels for in-situ bone formation in rat calvarial bone defects." Acta Biomaterialia **91**: 60-71.
Yanev, P., G. A. van Tilborg, A. van der Toorn, X. Kong, A. M. Stowe and R. M. Dijkhuizen (2022). "Prolonged release of VEGF and Ang1 from intralesionally implanted hydrogel promotes perilesional vascularization and functional recovery after experimental ischemic stroke." Journal of Cerebral Blood Flow & Metabolism **0**(0): 0271678X211069927.
Yang, B., X. Li, S. Shi, X. Kong, G. Guo, M. Huang, F. Luo, Y. Wei, X. Zhao and Z. Qian (2010). "Preparation and characterization of a novel chitosan scaffold." Carbohydrate Polymers **80**(3): 860-865.
Yang, P., Y. Zhang, L. Zhang, Y. Zhang, K. M. Treurniet, W. Chen, Y. Peng, H. Han, J. Wang, S. Wang, C. Yin, S. Liu, P. Wang, Q. Fang, H. Shi, J. Yang, C. Wen, C. Li, C. Jiang, J. Sun, X. Yue, M. Lou, M. Zhang, H. Shu, D. Sun, H. Liang, T. Li, F. Guo, K. Ke, H. Yuan, G. Wang, W. Yang, H. Shi, T. Li, Z. Li, P. Xing, P. Zhang, Y. Zhou, H. Wang, Y. Xu, Q. Huang, T. Wu, R. Zhao, Q. Li, Y. Fang, L. Wang, J. Lu, Y. Li, J. Fu, X. Zhong, Y. Wang, L. Wang, M. Goyal, D. W. J. Dippel, B. Hong, B. Deng, Y. B. W. E. M. Roos, C. B. L. M. Majoie and J. Liu (2020). "Endovascular Thrombectomy with or without Intravenous Alteplase in Acute Stroke." New England Journal of Medicine **382**(21): 1981-1993.
Zhang, N., J. He and F. Wu (2020). "Tuning the gelation behavior and cellular response of thermo-sensitive chitosan hydrogels." Materials Letters **260**: 126903.
Zhang, S. (2019). "Microglial activation after ischaemic stroke." Stroke and Vascular Neurology **4**(2): 71-74.
Zhao, S.-c., L.-s. Ma, Z.-h. Chu, H. Xu, W.-q. Wu and F. Liu (2017). "Regulation of microglial activation in stroke." Acta Pharmacologica Sinica **38**(4): 445-458.
Zhou, H. Y., L. J. Jiang, P. P. Cao, J. B. Li and X. G. Chen (2015). "Glycerophosphate-based chitosan thermosensitive hydrogels and their biomedical applications." Carbohydrate Polymers **117**: 524-536.
Zhou, L., C. Dai, L. Fan, Y. Jiang, C. Liu, Z. Zhou, P. Guan, Y. Tian, J. Xing, X. Li, Y. Luo, P. Yu, C. Ning and G. Tan (2021). "Injectable Self-Healing Natural Biopolymer-Based Hydrogel Adhesive

with Thermoresponsive Reversible Adhesion for Minimally Invasive Surgery." Advanced Functional Materials **31**(14): 2007457.